Joint International Conference on Supercomputing in Nuclear Applications and Monte Carlo 2013 (SNA + MC 2013)
La Cité des Sciences et de l'Industrie, Paris, France, October 27-31, 2013

Geant4 electromagnetic physics: improving simulation performance and accuracy

V. N. Ivanchenko[1,2,3*], S. Incerti[4], J. Allison[3], A. Bagulya[5], J. M. C. Brown[6], C. Champion[4], S. Elles[7], Z. Francis[8], V. Grichine[5], A. Ivantchenko[1,3], J. Jacquemier[7], M. Karamitros[4], M. Maire[3,7], A. Mantero[9], J. P. Marques[10,11], L. Pandola[12], M. Raine[13], M. A. Reis[10,14], G. Santin[15], D. Sawkey[16], A. Schaelicke[17], M. Schenk[18], A. Taborda[10,14], L. Urban[3] and T. Yamashita[19]

on behalf of the Geant4 Collaboration

[1] *CERN, CH1211 Geneva 23, Switzerland*
[2] *Ecoanalytica,119899 Moscow, Russia*
[3] *Geant4 Associates International Ltd, United Kingdom*
[4] *Université Bordeaux 1, CNRS/IN2P3, CENBG, 33175 Gradignan, France*
[5] *Lebedev Physics Institute, 119991 Moscow, Russia*
[6] *Monash University, School of Physics, Melbourne, Australia,*
[7] *LAPP, 74941 Annecy-le-vieux, France*
[8] *Université Saint Joseph, Faculty of Science, Department of Physics, Beirut, Lebanon*
[9] *INFN-Genova, 16146 Genova, Italy*
[10] *Centro de Física Atómica da Universidade de Lisboa, 1649-003 Lisboa, Portugal*
[11] *Departamento de Física da Faculdade de Ciências, Universidade de Lisboa, Campo Grande, Ed. C8, 1749-016 Lisbon, Portugal*
[12] *INFN-LNGS, 67100 Assergi, Italy*
[13] *CEA, DAM, DIF, F-91297 Arpajon, France*
[14] *IST/ITN, Instituto Superior Técnico, Universidade de Lisboa, Campus Técnológico e Nuclear, 2686-953 Sacavém, Portugal*
[15] *ESA/ESTEC, 2200 AG Noordwjik, The Netherlands*
[16] *Varian Medical Systems, Palo Alto, CA 94304, USA*
[17] *Helmholtz-Zentrum Berlin für Materialien und Energie GmbH, 12489 Berlin, Germany*
[18] *The University of Bern, LHEP, CH-3012 Bern, Switzerland*
[19] *Hyogo Ion Beam Medical Center, Tatsuno, Japan*

[*] Corresponding Author, E-mail: Vladimir.Ivantchenko@cern.ch

The most recent upgrades of the electromagnetic (EM) physics "standard" and "low energy" sub-libraries of the general purpose Geant4 Monte Carlo simulation toolkit are described. These upgrades are relevant to different application domains including high energy physics, medical physics and space science. Validation results are presented and discussed.

KEYWORDS: Monte Carlo, Geant4, electromagnetic physics.

I. Introduction

The Geant4 Monte Carlo general purpose toolkit[1, 2)] includes a large variety of physics models for the simulation of particle transport in matter. It covers a wide spectrum of application domains, including simulation of high energy physics experiments, beam transport, nuclear physics, radiation medicine, cosmic rays and radiation in space. Electromagnetic (EM) physics sub-libraries[3, 4)] of the toolkit are used practically in all types of simulations and determine the accuracy of many simulation predictions.

In this work we report on recent progress in electromagnetic physics in the Geant4 public release 9.6 (available since December 2012) and beta version of the new release 10.0 (available since June 2013). Some models and interfaces were upgraded, and new models have been added. The unification of all EM model interfaces has been completed. A new sub-library "dna" was created. A migration for EM models and processes was done for compatibility with Geant4 multi-threading (MT)[5)]. This paper presents both an overview of these new features, and new validation results.

II. Photon models

Models for photon interactions have been reviewed and improved. The interfaces to the angular generators were unified. All photo-electric effect and Compton scattering models were migrated to a common interface for the de-excitation module[6)], allowing the sharing of internal physics tables of photon models/processes between threads in MT mode.

A new model[7, 8)] (*G4LowEPComptonModel)* for Compton scattering has been developed by the Monash University group (Australia). This model was created to address the

limited accuracy of approximations utilised in sampling the ejected Compton electron direction seen in Geant4 and other photon transport simulation software[9-13]. It was developed from first principles[14] utilising a two-body fully relativistic three-dimensional scattering framework in the Relativistic Impulse Approximation for bound atomic electrons. Comparison of this new model with respect to the Compton scattering models of Livermore and Penelope shows a high level of agreement between the photon scattering algorithms of all three models[8]. However, the ejected Compton electron angular distributions of the Monash model exhibit a more realistic distribution than those of the Livermore and Penelope Compton scattering models[8]. An example of the extent of this difference can be seen in Fig. 1 which shows 2-D distribution for electron polar angle respect to the primary photon and azimuthal angle respect to the photon scattering plane. Experimental validation of the Monash Compton scattering model for the K-shell Compton scattering of 662 keV photons in gold is reported in Ref.[8].

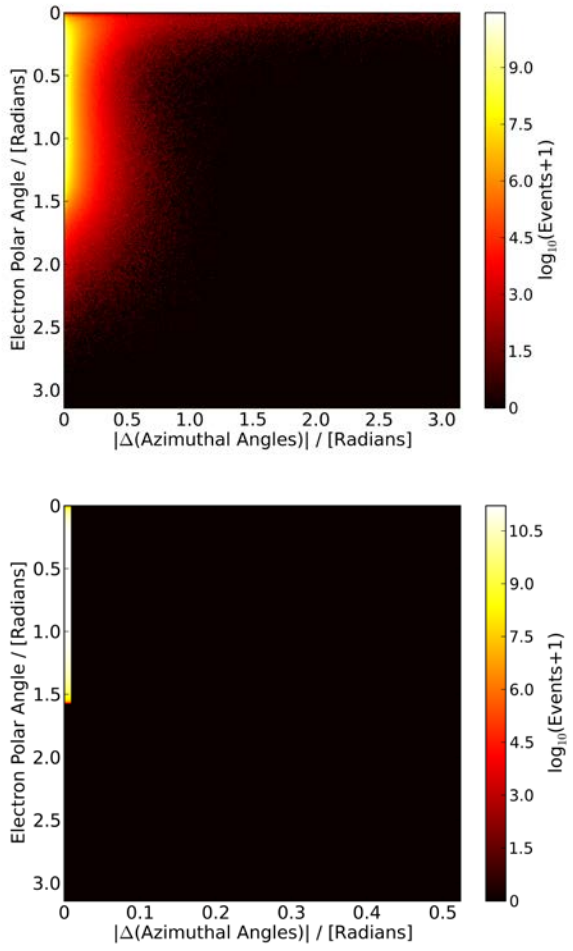

Figure 1: The Monash (top) and Penelope (bottom) model two-dimensional log intensity histograms of the ejected Compton electron angles for Cu at 500 keV photon beam.

Data management and sampling algorithms of the low energy Livermore models, including Rayleigh scattering, gamma conversion, photo-electric effect, and partial Compton scattering, have been optimised. These models are based on the EPDL data library[15] which is transformed into Geant4 G4LEDATA data sets. Internal data inside Livermore models were moved to standard Geant4 *G4PhysicsVector* and *G4ElementData* formats allowing sharing of these data between threads in MT mode. Low-energy limits were reduced to real EPDL values. High energy limits were extended by usage of asymptotic formulas for cross sections. Sampling algorithms for final states have been significantly updated. In particular, the Livermore Rayleigh scattering model is now 1000 times faster for energies above 100 keV, and can now be used in standard EM physics constructors. CPU performance of other Livermore models was also improved. In all Compton scattering and photo-electric effect models, a new general interface for de-excitation is introduced (see section VI). A summary of all recommended Geant4 photon models is shown in Table 1. The main difference between models is the sampling of the final state, at the same time the cross sections are similar for energies where compared models are applicable. Validation[16] of cross sections was performed versus NIST and other evaluated data-bases.

Model	E_{min}	E_{max}	CPU
G4LivermoreRayleighModel	100 eV	10 PeV	1.2
G4PenelopeRayleighModel	100 eV	10 GeV	0.9
G4KleinNishinaCompton	100 eV	10 TeV	1.4
G4KleinNishinaModel	100 eV	10 TeV	1.9
G4LivermoreComptonModel	100 eV	10 TeV	2.8
G4PenelopeComptonModel	10 keV	10 GeV	3.6
G4LowEPComptonModel	100 eV	20 MeV	3.9
G4BetheHeitlerModel	1.02 MeV	100 GeV	2.0
G4PairProductionRelModel	10 MeV	10 PeV	1.9
G4LivermoreGammaConversionModel	1.02 MeV	100 GeV	2.1
G4PenelopeGammaConversionModel	1.02 MeV	10 GeV	2.2
G4PEEFluoModel	1 keV	10 PeV	1
G4LivermorePhotoElectricModel	10 eV	10 PeV	1.1
G4PenelopePhotoElectricModel	10 eV	10 GeV	2.9

Table 1: List of recommended Geant4 photon models, applicability range, and relative CPU time for sampling of final state for 1 MeV gamma in Aluminum (10 MeV for gamma conversion) normalized to G4PEEFluoModel time.

III. Ionisation models

Models of ionisation are an essential part of charged particle transport code. Geant4 predicts hadron and ion transport with good accuracy[17]. Standard validation versus measurement is demonstrated in Fig.2 for protons in water for Geant4 10.0 beta. Note that for this Geant4 version management of internal tables for energy loss and range was changed due to the migration to MT providing sharing of all tables between threads. This internal reorganisation of tables does not affect physics results but slightly improves CPU and memory usage.

There are currently two models of energy loss straggling: the standard sub-library model (*G4UniversalFluctuations*) based on an empirical parameterisation[19] and the photo-absorption ionisation model[20] (PAI) which considers all ionisation collisions. The first model is the default, and the PAI model is recommended for accurate simulation in sensitive volumes.

Recently these models were updated in order to be applicable to thin solid targets and gaseous detectors. The results of comparison with the ALICE TPC test-beam data[21,22] (Fig.3) demonstrate that both models can provide satisfactory results; however, the PAI model is stable versus step size while the default model needs optimisation of step limits. The alternative PAI-Photon model for this case demonstrates the same performance as the PAI model. The PAI-Photon model samples not only delta-rays but also X-rays.

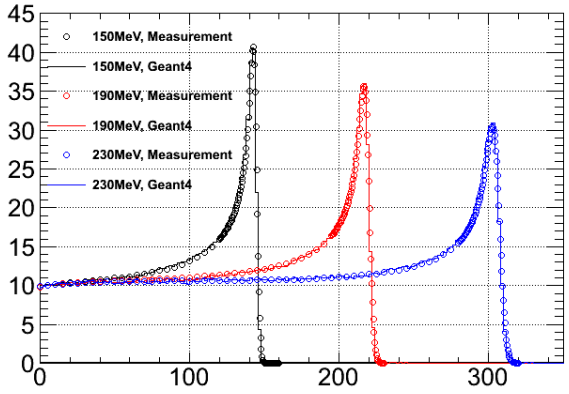

Figure 2: Proton Bragg peak shape in water (millimeters) for different energies of proton beam: histogram – simulation, open circles – data[18], 0.1 mm cut, Opt3 EM Physics List is used.

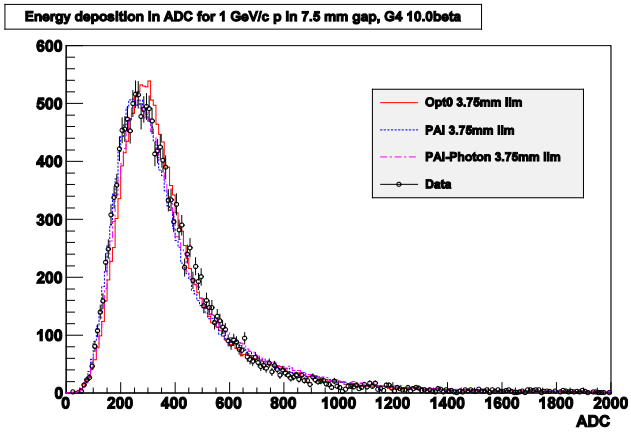

Figure 3: Proton energy deposition in gas gap in ADC counts: histogram – simulation, open circles – data[21,22], 1 mm cut, step limit is equal to half gap thickness, beam momentum is 1 GeV/c, gas mixture Ne–CO_2–N_2; ADC scale for simulation was normalized on the PAI model peak position.

New microdosimetry processes[23, 24] based on the dielectric formalism have been developed at CEA (France) specifically to model the transport and generation of very low energy (down to 5 eV) electrons by incident electrons, protons and heavy ions in silicon. The aim of these developments is to study the effect of ionizing radiation in highly integrated microelectronic components[25]. The size of current and future devices indeed requires a description of the deposited energy distribution at nanometric dimensions. For that, each ionisation collision should be simulated and condensed history algorithms (continues energy loss and multiple scattering) should not be applied. These new processes are fully included in the Geant4 public distribution since the 9.6 beta version, under the name "MuElec"[1].

The list of physical interactions per particle type that can be modeled using the "MuElec" processes and models is reported in Table 2. The corresponding process classes, model classes, low and high energy limits of applicability of models, and energy threshold below which the incident particle is killed (stopped and the kinetic energy is locally deposited) are also listed. All models are interpolated. For now, they are valid for Silicon only (requiring the use of the «G4_Si» Geant4-NIST material). Developments for other materials are foreseen.

Since the first version of "MuElec" described in refs.[23, 24] and released in 9.6 beta, the energy range of applicability has been extended from 50 keV up to 100 MeV for electrons and from 23 MeV/u up to 1 GeV/u for protons and heavy ions (release 9.6 and 10.0beta). Further extension is under progress to go up to 10 GeV/u for protons and heavy ions, while improving the proton stopping power evaluation (shown to be overestimated[25]). These improvements are summarized in Fig.4 which shows the relative difference of stopping powers calculated with SRIM[26] (software of reference for stopping power calculations), the first version of "MuElec" and the future one, compared to the PSTAR database[27]. A full description of these new developments will be given in a dedicated publication[28]. They are expected to be introduced in Geant4 in release 10.0.

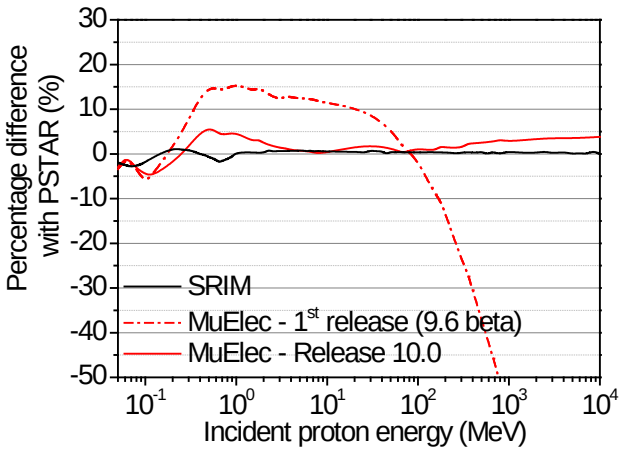

Figure 4: Percentage difference with PSTAR database[27] as a function of the incident proton energy for stopping powers calculated with the first version of MuElec (Geant4 release 9.6 beta) and the future one (release 10.0). The SRIM[26] comparison with PSTAR is also represented.

[1] "MuElec" stands for micro(μ)-electronics. The name will be changed to "MicroElec" in the release 10.0 of Geant4, to avoid any confusion with muon processes.

Process	Geant4 process class	Geant4 model class	E_{min}	E_{max}
Electrons				
Elastic scattering	G4MuElecElastic	G4MuElecElasticModel	5 eV (*)	100 MeV
Ionisation	G4MuElecInelastic	G4MuElecInelasticModel	16.7 eV	100 MeV
Protons and ions				
Ionisation	G4MuElecInelastic	G4MuElecInelasticModel	50 keV/u	1 GeV/u

Table 2: "MuElec" physical interactions per particle type, and corresponding Geant4 processes and models, with energy ranges of applicability; (*) denotes a tracking cut below this energy.

IV. Bremsstrahlung

The relativistic Landau-Pomeranchuk-Migdal effect (LPM) is taken into account at high energies in ultra-relativistic bremsstrahlung and gamma conversion models using a recent theory which was verified versus experimental data[29]. At moderate energies, a new *G4SeltzerBergerModel* was created within the standard EM sub-library[30]. This model uses a parameterisation based on evaluated data tables[31] of Seltzer and Berger. For these new models computation[3] of restricted energy loss and restricted cross sections is performed using numerical integration instead of empirical parameterisations used in previous models of the standard sub-library.

V. Multiple and single scattering

In recent years a set of Geant4 multiple scattering and single scattering models[32] was established. These models are tuned per particle type and application domain. In particular, single scattering models are useful for the sampling of charged particle transport in thin layers or low-density media. New single scattering models[33, 34] for space applications are available with Geant4 9.6.

Multiple scattering models determine CPU performance and accuracy of particle transport. For Geant4 9.6 sampling of scattering was moved from post-step to along-step before sampling of energy loss and straggling. This design change is an essential step in order to provide the possibility of sampling the lateral displacement of a charged particle on geometry boundary. For backward compatibility in Geant4 9.6 and in previous releases several versions of the Urban model[35] were delivered. Recent tuning of the model and analysis of validation results allows consolidation of the model into only one version for the release 10.0 (*G4UrbanMscModel*).

The validation was performed using the EM testing suite[36] which has been significantly extended for multiple and single scattering models[29, 30]. For electrons, multiple scattering models were tested by comparing simulations to electron scattering benchmark measurements[37]. The code used for the simulations is the *electronScattering2* extended example[38], available in the Geant4 distribution. Scattering from various thicknesses of 7 different materials with atomic numbers ranging from 4 to 79, for incident electron energies of 13 and 20 MeV, was simulated. The width of the central portion of the scattering peak was compared to measured values. This width was determined by a Gaussian fit to the part of the curve above 1/e of the peak height. These widths obtained from simulation, divided by the measured widths, are shown in Fig.5 for the standard EM Physics List *standard_option4* (Opt4). For 30 out of 35 points, widths are within 2% of the experimental value (the experimental uncertainty was 1%), with the worst disagreement of 3.5% for carbon.

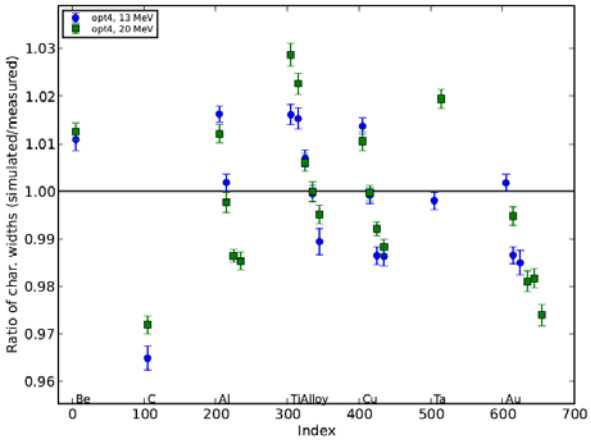

Figure 5: Ratio of simulated to measured scattering peak widths, as a function of scattering foil index. The index increases with increasing atomic number. The standard physics list Opt4 was used.

The overall goodness of fit was calculated using the chi-square method. This parameter takes into account the agreement at large scattering angles in addition to the central peak. The measured data were reported in N angular bins normalized to the first bin. Because of this, the simulated histograms were renormalized to minimize χ^2/N. Results are presented in Fig.6 for the Opt4 Physics List.

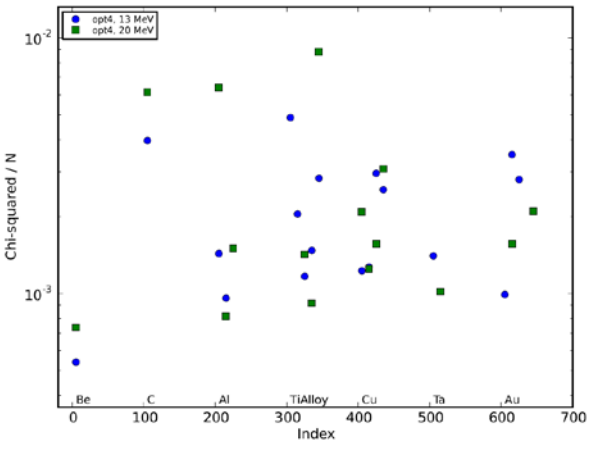

Figure 6: The value χ^2/N, used to compare the goodness of the simulation over the full range of measured scattering angles.

Thus, for electron transport the final version of the Urban model is the most accurate. Previous versions[38] demonstrated worse agreement. For other particle types and for high energies, the alternative combined approach[29, 30, 32] of the WentzelVI (WVI) multiple scattering model combined with the single scattering model has several advantages compared to the Urban model. First of all, these display the correct Rutherford tail of angular distribution for large scattering angles at any projectile energy, and a smaller dependence of the simulation results on step size. For low energy muons, it is confirmed by comparison with MuScat experimental data[39]. In Fig.7 values of χ^2/N are shown for 10 different targets and for sum over all available targets.

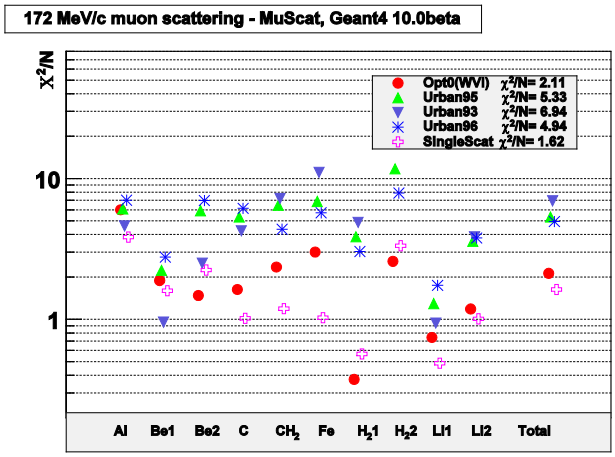

Figure 7: Comparison of simulation of muon scattering in different targets versus data[39]. The value χ^2/N for different versions of Urban model, WentzelVI model (WVI) and single scattering model. In the default EM Physics List Opt0 a combination WVI and single scattering is used.

Another new high energy benchmark provides comparison of transfer displacement of muon tracks[40] from Z-boson decay in muon system of L3 detector at CERN LEP collider. Experimental data compared with simulation predictions are shown in Table 3 which demonstrates that WVI and single scattering models are significantly closer to the data than old Urban models. Note that this benchmark is done using simplified geometry of the L3 detector. The most recent version of Urban model prediction is practically similar to the WVI prediction. Thus analysis of all available multiple scattering benchmarks allow to remove all old versions of the Urban model and release with Geant4 10.0 the most accurate one.

Model	Displacement (mm)
Urban90	7.639 ± 0.095
Urban93	6.989 ± 0.083
Urban95	6.630 ± 0.080
Urban96	6.442 ± 0.080
WentzelVI+Single Scattering	6.404 ±0.079
Data[40]	6.078 ± 0.028

Table 3: RMS of 45.6 GeV muon displacement in the muon system of L3 detector at the LEP collider.

VI. Atomic de-excitation

Since Geant4 9.6 all EM models and the radioactive decay model use the same common atomic de-excitation interface[6] which allows the simulation of radiative and non-radiative atomic relaxation (fluorescence X-rays and Auger electrons emission). Consequently, the de-excitation module is usable in all Geant4 electromagnetic physics constructors and is steered via standard Geant4 command line interface (UI) or via C++ interface. In particular, de-excitation module can be used for the simulation of fluorescence spectra obtained in particle induced X-ray emission (PIXE) elemental ion beam analysis experiments. In a recent study[41], sample targets were irradiated with a 3 MeV proton beam and the de-excitation spectra were detected using a Si(Li) detector. The obtained results were compared with Geant4 simulated X-ray spectra. Validation was done for mono-elemental samples of Si, Al, Cu and Fe and more complex reference samples containing more than ten elements, e.g. B-EN and stainless steel (see details in[41]). Figure 8 shows an example of comparison of the copper K-shell de-excitation simulated with Geant4 and the experimental data.

In the updated de-excitation module PIXE simulation is performed generically using shell ionisation cross sections interface. Models of ionization are responsible only for simulation of energy loss and delta-electron emission. Users may define cross section class per particle type, with default cross sections provided. For hadrons and heavy ions, original shell cross sections are not available; in that case scaling from the proton one is used. Additional shell ionisation cross sections for incident protons and alpha particles for K, L and M shells have been recently added for the simulation of PIXE. These models cover the 100 keV – 100 MeV incident energy range for K and L shells and for Z=6 to Z=92 target atomic numbers, and the 100 keV – 10 MeV range for M shells and for Z>61 up to Z=92 elements[42, 43]. These models, as well as the already existing set of empirical models and analytical models[6], are fully selectable using UI commands in Geant4 applications.

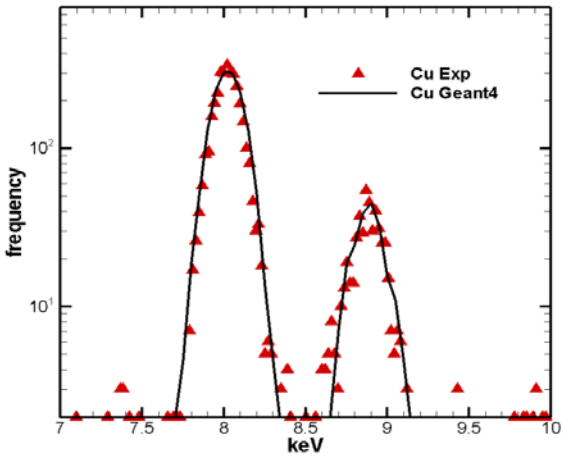

Figure 8: Energy of photons (K-shell radiation) from 3 MeV proton beam off thin copper target: red markers - experimental data; line - Geant4 simulation. Livermore EM physics list was used. Detector resolution is taken into account.

VII. Geant4 DNA processes and models

Since 2007, Geant4 is being extended in the framework of the Geant4-DNA project[44] in order to provide an open-source platform able to simulate early DNA damage resulting from irradiation of biological samples, such as biological cells. All these Geant4-DNA developments are included in the new "dna" electromagnetic sub-library of Geant4. The simulation is based on a succession of the following three stages:

a) the "physical" stage where the interaction between ionizing radiation and the biological medium is simulated;
b) the "physico-chemical" stage where water - the main component of biological materials - impacted by ionizing radiation from previous stage may dissociate into new chemical species;
c) the "chemical" stage where chemical species may react either with each other, producing a temporal evolution of their concentrations, or with biological molecules such as DNA, leading to DNA damage.

For the "physical" stage, the Geant4-DNA extension provides a set of processes and models, which can reach the eV scale and simulate all discrete interactions in liquid water. Table 4 shows the list of processes and models currently available in Geant4-DNA.

In the context of the Geant4-DNA project, a prototype for simulating radiation chemistry of liquid water in Geant4 is currently being developed[45,46]. This module aims at simulating, at the biological cell scale, the chemical reactions occurring in the "chemical" stage from 1 picosecond up to 1 microsecond after irradiation. Its first version is based on the particle-continuum representation where each chemical species is explicitly simulated and the solvent is treated as a continuum and uses the diffusion-controlled reaction model. A full description of the implemented method and model can be found in ref.[46].

To benchmark radiochemistry codes, one of the criteria often used is the so-called time-dependent radiochemical yield. It corresponds, for a given chemical species, to the number of molecules available in the liquid water medium at a given time and for 100 eV of deposited energy:

$$G(t) = N(t)/100 \text{ eV}.$$

The time-dependent radiochemical yields of the two main radical species, namely the hydroxyl radical and the solvated electron, are reported for the case of irradiation with 1 MeV electrons. The simulated setup is an infinite water box. The radiochemical yields are computed for each single primary particle independently. When the primary particle has deposited more than 10 keV, it is withdrawn from the simulation. All its secondary electrons are followed until thermalization (i.e. when they reach the energy given by the medium's temperature, around 25 meV in our case) and solvation. The simulation of the "chemical" stage was done using the parameters given in[47] and the simulation method described in[48]. The results are presented in Fig.9. A full discussion of those results is given in[49].

We expect to deliver a first example user application called "dnachemistry" that will detail how to enable the chemistry stage of Geant4-DNA in the Geant4 release version 10.0 in December 2013. This example will show the user how to follow in time the evolution of the chemical reactions resulting from water irradiation.

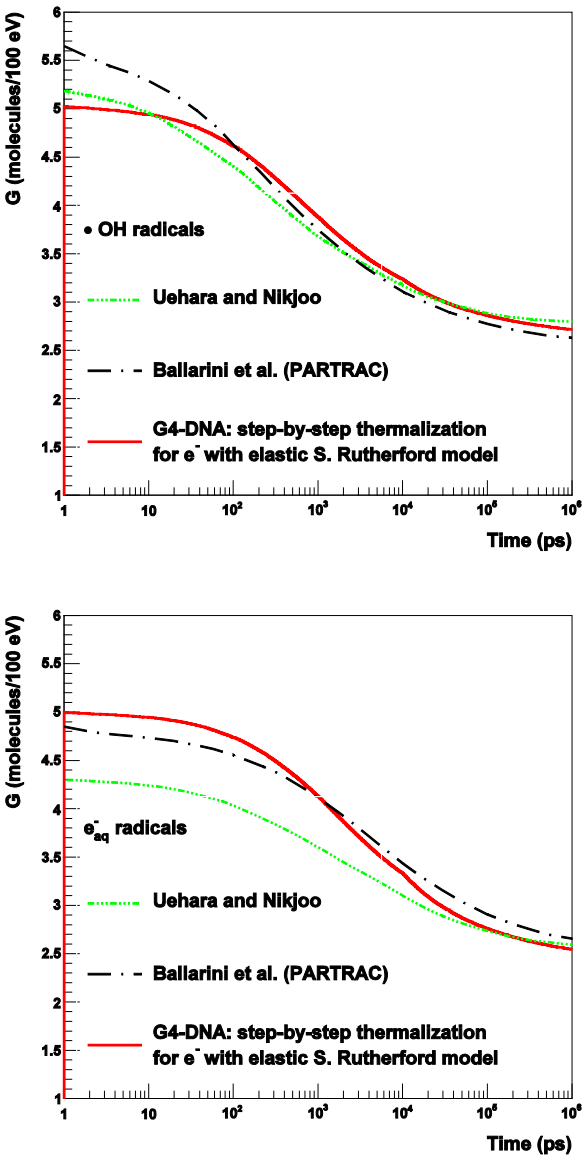

Figure 9: Time-dependent radiochemical yields for hydroxyl radicals (top) and solvated electrons (bottom). The red line is obtained using Geant4-DNA and is compared to the results in black obtained from Ballarini et al. (using the PARTRAC software)[48] and to the results in green obtained from Uehara and Nikjoo[49].

VIII. Built-in biasing options

For the first time, built-in EM biasing options are available inside the Geant4 toolkit. Geant4 version 9.6 includes: cross section biasing, forced interactions, splitting of final state, and Russian roulette. These biasing options may be enabled via UI command or C++ interfaces and can be applied on top of any EM Physics configurations. Cross section biasing may be useful to study the effects of uncertainty of EM cross sections on EM shower shape or other observables. Forced

interaction method is implemented only for the limited use-case of thin target assuming that forced interaction happens uniformly in the volume of interest and no correction is applied to secondary particle weight.
The other two methods are classical variance reduction techniques used to speed up simulation. Secondary particle splitting allows enhance secondary particle spectra in an area of interest. Russian roulette method is applicable for the case when too many secondary particles are produced (EM shower), so only a fraction of secondary particles is tracked with increased weight of each tracked particle.
The secondary particle splitting has been implemented in view of medical and other applications. The user may request that each interaction produce N secondaries, each of weight 1/N. Each secondary is chosen independently from the relevant distributions. The energy and momentum of the primary particle after scattering are determined from the first secondary (this preserves straggling). The splitting is configurable by Geant4 EM process type, geometry region, and energy interval for secondary particles.

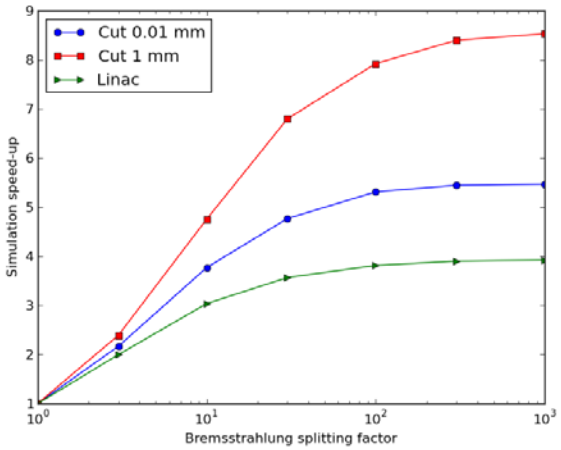

Figure 10: Relative speed-ups for the simulations, as a function of bremsstrahlung splitting factor. The product of number of incident particles and bremsstrahlung splitting factor was kept constant for each series of simulations. For curves labeled `Cut', 6 MeV electrons are shot onto on a W target. Production cuts of 0.01 and 1 mm were used, as labeled. For the curve labeled `Linac', a medical linear accelerator was simulated.

An example application involves medical linear accelerators with photon beams produced by bremsstrahlung. A large fraction of the simulation time can be spent simulating electron transport in the bremsstrahlung target. This may be reduced by creating multiple photons for each bremsstrahlung event. Fig.10 shows the speed-up of simulations, when the product of number of incident particles and the bremsstrahlung splitting factor is kept constant. Two geometries were considered: one was a 2 mm thick W target, with a 6 MeV incident electron beam. The second was a medical linear accelerator[50] operated at 6 MV (6.18 MeV incident electron beam). Relative simulation times decreased for both geometries with increasing bremsstrahlung splitting factors, up to a maximum improvement in speed of 8.5. The improvement in speed was greater for the simple geometry, reflecting the time spent transporting photons in the more complex geometry of the medical linear accelerator. Similarly, reducing the production cuts decreased the effectiveness of bremsstrahlung.

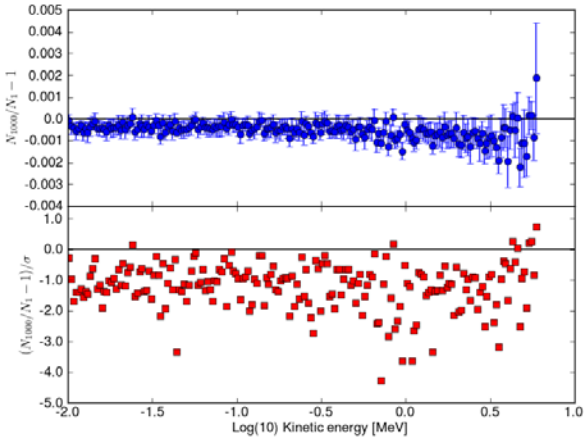

Figure 11: Ratio of number of photons (N) created for the simulation with splitting factor of 1000, to that with splitting factor 1, as a function of the kinetic energy of the photon. Lower curve shows the ratio relative to the statistical precision (σ).

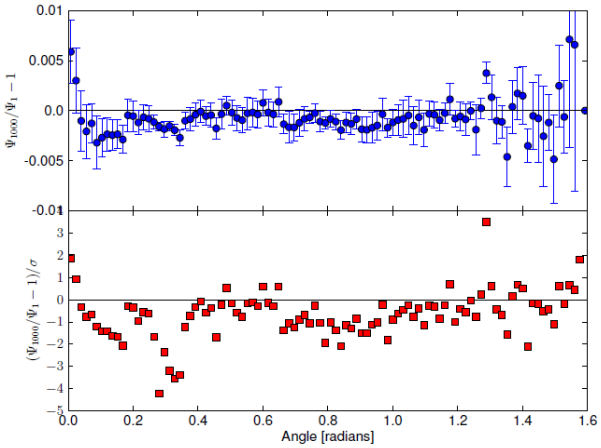

Figure 12: Ratio of the energy fluence (ψ) of photons leaving the target for simulations with bremsstrahlung splitting factors of 1000 and 1, as a function of the angle. Lower curve shows the ratio relative to the statistical precision (σ).

The accuracy of the bremsstrahlung splitting was evaluated by comparing the photons generated from simulations with different bremsstrahlung splitting factors. The example code *TestEm5* from Geant4 distribution was used, with a geometry consisting of a pencil beam of 6 MeV electrons on a 3 mm thick W target. Bremsstrahlung splitting factors of 1 (no splitting) and 1000 were used. The energy of the photons at their creation, plus the energy fluence, differential in angle, of photons exiting the target was recorded. All photons were considered, not just those created by bremsstrahlung. The ratio of these quantities for these two different bremsstrahlung splitting factors is expected to be 1. In Fig.11 the ratio of the number of photons per energy bin is shown. Results with the two different bremsstrahlung

splitting factors agreed to better than 0.05%. The lower panel of the figure shows the difference relative to the statistical uncertainty. In Fig.12 the energy fluence per angle bin is shown, and the agreement is 0.1% over most of the angular region. Agreement for both values is equal to the statistical uncertainty.

IX. Infrastructure of electromagnetic physics

With the release 9.6 the unification of all EM physics sub-libraries has been achieved for "standard", "low-energy", and "dna" sub-libraries. This allows combining models from different sub-libraries in EM physics constructors. For Geant4 9.6 in EM components[4] of physics lists have been updated. In all EM constructors (except standard Opt3) the WentzelVI multiple scattering model is used for electrons and positrons above 100 MeV, and for muons and hadrons at all energies. The Urban model is used below 100 MeV for electrons and positrons, and for all energies for ions. In standard Opt3 constructor Urban model is used for all particles at all energies. In all EM constructors the ultra-relativistic gamma conversion model is applied above 80 GeV. This model takes into account LPM effect providing more accurate high energy cross section.

A new physics constructor (standard Option4) has been designed in order to provide the most accurate EM physics to Geant4 users. For that, step limitation parameters are optimised per particle type and the most accurate models for gamma and electron transport from the "standard" and "low-energy" sub-libraries are used.

For the version 10.0 EM processes and models are adopted for the MT approach[5]: tables of energy loss, ranges, and cross sections are filled at initialisation time in the master thread and are available in the run time shared between all worker threads. This was achieved by migration of material property classes, 1-D and 2-D physics vector classes of Geant4 to read-only run time mode.

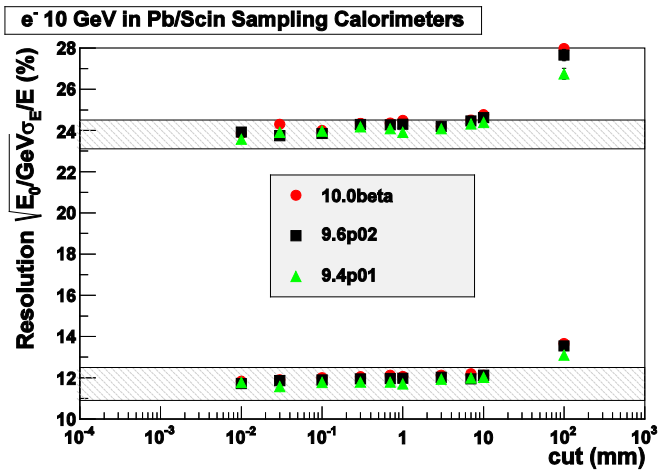

Figure 13: Energy resolution of two sampling Lead/Scintillator calorimeters for 10 GeV electrons: points – Geant4 simulation for different versions of the toolkit, hashed area – one standard deviation for the data[51, 52].

In Fig.13 resolution of two sampling calorimeters[51, 52] versus cut in range value[3] and Geant4 version is shown. A recommended cut in range for typical high energy calorimeters is 1 mm – Geant4 simulated energy resolution is at a plato while CPU performance is acceptable. For lower cut values required CPU time significantly increased. This plot illustrates good agreement of Geant4 simulation predictions with the data and stability of simulation results for high energy physics applications between Geant4 versions.

X. Summary

With the Geant4 version 9.6 the program of design change toward modularisation[3] and unified interfaces[4] was completed. This allowed straightforward migration of EM physics sub-libraries to Geant4 MT[5] and continues development of new high-energy, low-energy and DNA models. Geant4 EM physics is used successfully in many application domains, in particular, for simulation of experiments at Large Hadron Collider at CERN for discovery of Higgs boson[53, 54].

Acknowledgment

This work was supported in part by ESA TRP contracts 22712/09/NL/AT, 22839/10/NL/AT, and 4000107387/12/NL/AK.

References

1) S. Agostinelli et al., "Geant4 – a simulation toolkit," Nucl. Instr. Meth. A, 506, 250 (2003).
2) J. Allison et al., "Geant4 developments and applications," IEEE Trans. Nucl. Sci., 53, 270 (2006).
3) J. Apostolakis et al., "Geometry and physics of the Geant4 toolkit for high and medium energy applications," Rad. Phys. Chem., 78, 859 (2009).
4) V.N. Ivanchenko et al., "Recent improvements in Geant4 electromagnetic physics and interfaces," *Progress in Nuclear Science and Technology*, **2,** 898-903 (2011).
5) S. Ahn, J. Apostolakis, M. Asai, D. Brandt, G. Cooperman, G. Cosmo, A. Dotti, X. Dong, A. Novak and S. Y. Jun "Geant4-MT: bringing multi-threaded Geant4 into production", in these proceedings.
6) A. Mantero, H. Ben Abdelouahed, C. Champion, Z. El Bitar, Z. Francis, P. Guèye, S. Incerti, V. Ivanchenko, M. Maire, "PIXE simulation in Geant4," *X-Ray Spectrometry*, **40,** 135-140 (2011).
7) J.M.C. Brown, M.R. Dimmock, J.E. Gillam, D.M. Paganin, "MULECS: The Monash University Low Energy Compton scattering package," *proceedings of the Nuclear Science Symposium and Medical Imaging Conference (NSS/MIC) 2011*, pp. 1385-1389 (2011).
8) J.M.C. Brown, M.R. Dimmock, J.E. Gillam, D.M. Paganin, "A low energy bound atomic electron Compton scattering model for Geant4," *Nucl. Instr. Meth A*, in Review.
9) Y. Namito S. Ban and H. Hirayama, "Implementation of Doppler broadening of a Compton scattering photon into EGS4 code," *Nucl. Instr. Meth. A*, **349,** 489-494 (1994).
10) D. Brusa, G. Stutz, J. A. Riveros, J. M. Fernandes-Varea and F. Salvat, "Fast sampling algorithm of the simulation of

photon Compton scattering," *Nucl. Instr. Meth. A,* **379,** 167-175 (1996).
11) I. Kawrakow, D. W. O. Rogers, "The EGSnrc Code System: Monte Carlo Simulation of Electron and Photon Transport," NRCC Report PIRS-701, NRC, Otawa, 2001.
12) RSICC Computer Code Collection, MCNPX 2.4.0," Report CCC-715, LANL, Los Alamos, 2002.
13) M. R. Kippen, "The GEANT low energy Compton scattering (GLESC) package for the use in simulating advanced Compton telescopes," *New Astro. Reviews*, **48,** 221-225 (2004).
14) R. Ribberfors, "Relationship of the relativistic Compton cross section to the momentum distribution of bound electron states," *Phys. Rev. B,* **12,** 2067-2074 (1975).
15) D. Cullen, J.H. Hubbell, L. Kissel, "The evaluated photon data library," Report UCRL-50400, Vol.6 (1997).
16) G.A.P. Cirrone et al., "Validation of the Geant4 electromagnetic photon cross-sections for elements and compounds," *Nucl. Instr. Meth. A,* **618,** 315-322 (2010).
17) A. Lechner, V. N. Ivanchenko, J. Knobloch, "Validation of recent Geant4 physics models for application in carbon ion therapy," *Nucl. Instrum. and Meth. B,* **268,** 2343-2354 (2010).
18) Y. Kumazaki, T. Akagi, T. Yanou, D. Suga, Y. Hishikawa, T. Teshima, "Determination of the mean excitation energy of water from proton beam ranges", *Radiation Measurements*, 42, 1683 – 1691 (2007).
19) K. Lassila-Perini, L.Urban, "Energy loss in thin layers in GEANT," *Nucl. Instr. Meth. A,* **362,** 416 (1995).
20) V. Grichine et al., "An implementation of ionisation energy loss in very thin absorbers for the Geant4 simulation package," *Nucl. Instr. Meth. A,* **453,** 597-605 (2000).
21) D. Antonchyk et al., "Performance studies with an ALICE TPC prototype," *Nucl. Instr. Meth. A,* **565,** 551-560 (2006).
22) P. Christiansen, "Particle Identification Studies with an ALICE Test TPC," *Int. J. Mod. Phys. E,* **16,** 2457-2462 (2007).
23) A. Valentin, M. Raine, J.-E. Sauvestre, M. Gaillardin and P. Paillet, "Geant4 physics processes for microdosimetry simulation: very low energy electromagnetic models for electrons in silicon," *Nucl. Instr. Meth. B*, **288**, 66-73 (2012).
24) A. Valentin, M. Raine, M. Gaillardin and P. Paillet, "Geant4 physics processes for microdosimetry simulation: very low energy electromagnetic models for protons and heavy ions in silicon," *Nucl. Instr. Meth. B*, **287**, 124-129 (2012).
25) M. Raine, A. Valentin, M. Gaillardin and P. Paillet, "Improved simulation of ion track structures using new Geant4 models - Impact on the modeling of advanced technologies response ", *IEEE Transactions on Nuclear Science*, vol. 59, pp. 2697-2703, 2012.
26) SRIM [Online]. Available: http://www.srim.org
27) M. J. Berger, J. S. Coursey, M. A. Zucker and J. Chang, "NISTIR-4999: Stopping power and range tables for electrons, protons and helium ions", NIST Reports, 2005.
28) M. Raine, M. Gaillardin and P. Paillet, "Geant4 physics processes for Silicon microdosimetry simulation: improvements and extension of the energy-range validity up to 10 GeV/nucleon", *Nucl. Instr. Meth. B*, to be published.
29) A. Schaelicke, A. Bagulya, O. Dale, F. Dupertuis, V. Ivanchenko, O. Kadri, A. Lechner, M. Maire, M. Tsagri and L. Urban, "Geant4 electromagnetic physics for the LHC and other HEP applications," *J. Phys: Conf. Ser.,* **331,** 032029 (2011).
30) J. Allison, J. Apostolakis, A. Bagulya, C. Champion, S. Elles, F. Garay, V. Grichine, A. Howard, S. Incerti, V. Ivanchenko, J. Jacquemier, M. Maire, A. Mantero, P. Nieminen, L. Pandola, G. Santin, D. Sawkey, A. Schaelicke, and L.Urban, "Geant4 electromagnetic physics for high statistic simulation of LHC experiments," *J. Phys: Conf. Ser*., **396,** 022013 (2012).
31) S.M. Seltzer and M. J Berger, "Bremsstrahlung spectra from electron interactions with screened atomic nuclei and orbital electrons," *Nucl. Instrum. Meth. B,* **12,** 95 (1985).
32) 5) V.N. Ivanchenko, O. Kadri, M. Maire and L. Urban, "Geant4 models for simulation of multiple scattering", *J. Phys., Conf. Ser*., **219,** 032045 (2010).
33) M. J. Boschini, et al., "Nuclear and non-ionizing energy-loss for Coulomb scattered particles from low energy up to relativistic regime in space radiation environment". In: Giani, S., Leroy, C., Rancoita, P.G. (Eds.), Proceedings of the 12th ICATPP, 7–8 October 2010, Villa Olmo, Como, Italy. World Scientific, Singapore, pp. 9–23, ISBN: 978-981-4329-02-6 (2010).
34) M. J. Boschini et al., "An expression for the Mott cross section of electrons and positrons on nuclei with Z up to 118,"*Rad. Phys. Chem.*, **90,** 39-66 (2013).
35) L. Urban, "A multiple scattering model in Geant4," Preprint CERN-OPEN-2006-077 (2006).
36) J. Apostolakis, A. Bagulya, S. Elles, V.N. Ivanchenko, J. Jacquemier, M. Maire, T. Toshito and L. Urban, "Validation and verification of Geant4 standard electromagnetic physics," *J. Phys: Conf. Ser.*, **219,** 032044 (2010).
37) C. Ross et al., "Measurement of multiple scattering of 13 and 20 MeV electrons by thin foil," *Med. Phys*., **35,** 4121 (2008).
38) B.A. Faddegon et al., "The accuracy of EGSnrc, Geant4 and PENELOPE Monte Carlo systems for the simulation of electron scatter in external beam radiotherapy," *Phys. Med. Biol.,* **54**, 6151 (2009).
39) D. Attwood et al,. "The scattering of muons in low-Z materials," *Nucl. Instr. Meth. B,* **251,** 41 (2006).
40) P. Arce et al. "Multiple scattering in GEANT4. A comparison with Moliere theory and L3 detector data", Proceedings of MC-2000 Conference, EXP CERN-LEP-L3, (2000).
41) Z. Francis, M. El Bast, R. El Haddad, A. Mantero, S. Incerti, V. Ivanchenko, Z. El Bitar, C. Champion, M.A. Bernal, M. Roumie, "A comparison between Geant4 PIXE simulations and experimental data for standard reference samples," *Nucl. Instr. Meth. B,* in press (2013).
42) A. Taborda, P. C. Chaves, M. A. Reis, "Polynomial approximation to universal ionisation cross-sections of K and L shells induced by H and He ion beams," X-Ray Spectrometry, **40**, 127-134 (2011).
43) A. Taborda, P. C. Chaves, M. L. Carvalho, M. A. Reis, "Polynomial approximation to universal M-shell ionisation cross-sections induced by H+ and He2+ ions," *X-Ray Spectrometry*, **42**, 177-182 (2013).
44) S. Incerti, G. Baldacchino, M. Bernal, R. Capra, C. Champion, Z. Francis, P. Guèye, A. Mantero, B. Mascialino, P. Moretto, P. Nieminen, C. Villagrasa, C. Zacharatou, "The Geant4-DNA Project," *International Journal of Modeling, Simulation, and Scientific Computing*, **01**, 157-178 (2010).
45) M. Karamitros, A. Mantero, S. Incerti, G. Baldacchino, P. Barberet, M. Bernal, R. Capra, C. Champion, Z. El Bitar, Z. Francis, W. Friedland, P. Guèye, A. Ivanchenko, V. Ivanchenko, H. Kurashige, B. Mascialino, P. Moretto, P. Nieminen, G. Santin, H. Seznec, H. N. Tran, C. Villagrasa, C. Zacharatou, "Modeling radiation chemistry in the Geant4 Toolkit," *Progress in Nuclear Science and Technology*, **2**, 503-508 (2011).
46) M. Karamitros, S. Luan, M.A. Bernal, J. Allison, G. Baldacchino, M. Davidkova, Z. Francis, W. Friedland, V. Ivantchenko, A. Ivantchenko, A. Mantero, P. Nieminem, G. Santin, V. Stepan, N.H. Tran, S. Incerti, "Improving

computational performance of the chemistry module of Geant4-DNA," submitted (2013).
47) V. Breton, C. Champion, Z. El Bitar, M. Karamitros, S. B. Lee, L. Maigne, Y. Perrot, Q. T. Pham, J. I. Shin, H. N. Tran, S. Incerti, "Extended Geant4 at the physics-medicine-biology frontier", submitted (2013).
48) S. Uehara, H. Nikjoo, "Monte Carlo Simulation of Water Radiolysis for Low-energy Charged Particles", *Journal of Radiation Research*, **47**, 69-81 (2006).
49) F. Ballarini, M. Biaggi, M. Merzagora, A. Ottolenghi, M. Dingfelder, W. Friedland, P. Jacob, H.G. Paretzke, "Stochastic aspects and uncertainties in the prechemical and chemical stages of electron tracks in liquid water: a quantitative analysis based on Monte Carlo simulations," *Radiation and Environmental Biophysics*, **39**, 179-188 (2000).
50) M. Constantin et al., "Modeling the TrueBeam linac using a CAD to Geant4 geometry implementation: Dose and IAEA-compliant phase space calculations," *Med. Phys.*, **38,** 4018 (2011).
51) E. Bernardi E et al, „Performance of a compensating lead-scintillator hadronic calorimeter," *Nucl. Instrum. Meth. A*, **262**, 229-242, (1987).
52) G. D'Agostini et al., "Experimental study ofuranium plastic scintillator calorimeters," *Nucl. Instrum. Meth. A*, **274**, 134, (1989).
53) ATLAS Collaboration, "Observation of a new particle in the search for the Standard Model Higgs boson with the ATLAS detector at the LHC", *Phys. Lett. B* **716**, 1-29, (2012).
54) CMS Collaboration, "Observation of a new boson at a mass of 125 GeV with the CMS experiment at the LHC", *Phys. Lett. B*, **716**, 30-61, (2012).

Process	Geant4 process class	Geant4 model class	E_{min}	E_{max}
Electrons				
Elastic scattering	G4DNAElastic	G4DNAScreenedRutherfordElasticModel	9 eV(*)	1 MeV
		G4DNAChampionElasticModel	7.4 eV(*)	1 MeV
Excitation	G4DNAExcitation	G4DNABornExcitationModel	9 eV	1 MeV
Ionisation	G4DNAIonisation	G4DNABornIonisationModel	11 eV	1 MeV
Vibrational excitation	G4DNAVibExcitation	G4DNASancheExcitationModel	2 eV	100 eV
Attachment	G4DNAAttachment	G4DNAMeltonAttachmentModel	4 eV	13 eV
Protons				
Excitation	G4DNAExcitation	G4DNAMillerGreenExcitationModel	10 eV	500 keV
		G4DNABornExcitationModel	500 keV	100 MeV
Ionisation	G4DNAIonisation	G4DNARuddIonisationModel	100 eV(*)	500 keV
		G4DNABornIonisationModel	500 keV	100 MeV
Charge decrease	G4DNAChargeDecrease	G4DNADingfelderChargeDecreaseModel	100 eV	100 MeV
Hydrogen				
Excitation	G4DNAExcitation	G4DNAMillerGreenExcitationModel	10 eV	500 keV
Ionisation	G4DNAIonisation	G4DNARuddIonisationModel	100 eV(*)	100 MeV
Charge increase	G4DNAChargeIncrease	G4DNADingfelderChargeIncreaseModel	100 eV	100 MeV
Neutral helium ionised twice				
Excitation	G4DNAExcitation	G4DNAMillerGreenExcitationModel	1 keV	400 MeV
Ionisation	G4DNAIonisation	G4DNARuddIonisationModel	1 keV(*)	400 MeV
Charge decrease	G4DNAChargeDecrease	G4DNADingfelderChargeDecreaseModel	1 keV	400 MeV
Neutral helium ionised once				
Excitation	G4DNAExcitation	G4DNAMillerGreenExcitationModel	1 keV	400 MeV
Ionisation	G4DNAIonisation	G4DNARuddIonisationModel	1 keV(*)	400 MeV
Charge decrease	G4DNAChargeDecrease	G4DNADingfelderChargeDecreaseModel	1 keV	400 MeV
Charge increase	G4DNAChargeIncrease	G4DNADingfelderChargeIncreaseModel	1 keV	400 MeV
Neutral helium				
Excitation	G4DNAExcitation	G4DNAMillerGreenExcitationModel	1 keV	400 MeV
Ionisation	G4DNAIonisation	G4DNARuddIonisationModel	1 keV(*)	400 MeV
Charge increase	G4DNAChargeIncrease	G4DNADingfelderChargeIncreaseModel	1 keV	400 MeV
C, N, O, Fe ions				
Ionisation	G4DNAIonisation	G4DNARuddIonisationExtendedModel	1 keV(*)	400 MeV

Table 4: **List of Geant4 very low energy processes and models available in the Geant4-DNA extension (Geant4 version 9.6p02) for track structure simulation in liquid water during the "physical" stage. Low and high-energy limit applicability of models are shown. (*) denotes a tracking cut below the corresponding kinetic energy.**